GEOPHYSICS®

Wave simulation in double-porosity media based on the Biot-Rayleigh theory

Journal:	*Geophysics*
Manuscript ID	GEO-2018-0575.R1
Manuscript Type:	Hydromechanical Phenomena at the Pore Scale and their Upscaling
Keywords:	attenuation, modeling, viscoelastic, wave propagation, dispersion
Area of Expertise:	Seismic Modeling and Wave Propagation

Geophysics, manuscript No.
(will be inserted by the editor)

Wave simulation in double-porosity media based on the Biot-Rayleigh theory

Enjiang Wang[2] · José M. Carcione[1,2] · Jing Ba[2]

the date of receipt and acceptance should be inserted later

Right-running head: Wave simulation in double-porosity media

Abstract We develop a numerical algorithm for simulation of wave propagation in double-porosity media, where the pore space is saturated with a single fluid. Spherical inclusions embedded in a background medium oscillate to yield attenuation by mode conversion from fast P-wave energy to slow P-wave energy (mesoscopic or wave-induced fluid-flow loss). The theory is based on Biot theory of poroelasticity and the Rayleigh model of bubble oscillations. The differential equation of the Biot-Rayleigh (BR) variable is approximated with the Zener mechanical model, which results in a memory-variable viscoelastic equation. These approximations are required to model mesoscopic losses arising from conversion of the fast P-wave energy to slow diffusive modes. The model predicts a relaxation peak in the seismic band, depending on the diameter of the patches, to model the attenuation level observed in rocks. The wavefield is obtained with a grid method based on the Fourier differential operator and a second-order time-integration algorithm. Since the presence of

[1]Istituto Nazionale di Oceanografia e di Geofisica Sperimentale (OGS), Borgo Grotta Gigante 42c, 34010 Sgonico, Trieste, Italy. E-mail: jcarcione@inogs.it
[2] School of Earth Science and Engineering, Hohai University, Nanjing, 211100, China.

two slow quasi-static modes makes the differential equations stiff, a time-splitting integration algorithm is used to solve the stiff part analytically. The modeling has spectral accuracy in the calculation of the spatial derivatives.

Keywords wave simulation · double porosity · Biot-Rayleigh theory · Zener model · pseudospectral method

Introduction

The theory of wave propagation in porous media has multiple applications in different fields, notably in hydrocarbon exploration (e.g., Müller et al., 2010). Since Biot's initial work (Biot, 1956), many generalizations have been performed, including two fluids (Santos et al., 1990), two solids (Carcione and Seriani, 2001) and double porosity (Pride et al., 2004; Ba et al., 2011).

The Lagrangian formulation of Ba et al. (2011), based on a combination of Biot's theory and Rayleigh's model of oscillating bubbles, holds for uniform (constant) porosity, since they use the average displacements of the solid and fluid phases as Lagrangian coordinates, and the respective stress components as conjugate variables. Biot (1962) proposes as generalized coordinates the displacements of the solid matrix and the variation of fluid content. In this case, the corresponding conjugate variables are the total stress components and the fluid pressure. Here, we generalize the double-porosity equations of Ba et al. (2011) to non-uniform (variable) porosity using a similar approach.

Simulation of synthetic seismograms in the presence of mesoscopic loss requires solving the corresponding differential equations. Because the loss mechanism involves the conversion of fast P-wave energy to diffusion energy in the form of two slow waves and the wavelength of these waves can be very small, the poroelastic solution requires a very large amount of storage and computer time. An efficient approach is to approximate the attenuation and velocity dispersion curves using a viscoelastic rheology (Carcione, 1998; Picotti et al., 2010; Picotti and Carcione, 2017).

The Biot-Rayleigh (BR) differential equations are of the form $\dot{\mathbf{v}} = \mathbf{M}\mathbf{v}$, where $\mathbf{v}$ is the field vector and $\mathbf{M}$ is the propagation matrix (the dot denotes time differentiation). As in the poroacoustic case (Carcione and Quiroga-Goode, 1995) all the eigenvalues of $\mathbf{M}$ have negative real part. While the eigenvalues of the fast waves have a small real part (in absolute value), the eigenvalues of the slow waves (in the quasi-static regime) have a large real part. The presence of these quasi-static modes makes the differential equations *stiff*. Thus, seismic and sonic modeling are unstable when using explicit time integration methods. Carcione and Quiroga-Goode (1995) and Carcione and Seriani (2001) solved this problem by using a splitting or partition method.

In this work, we do not replace the differential equations with the viscoelastic equations as in Carcione (1998) and Picotti et al. (2010) but keep the explicit poroelastic formulation. The attenuation characteristic of wave propagation in the seismic band are approximated with a Zener mechanical model for the bulk modulus (e.g., Carcione, 2014), which provides a perfect fit of the BR mesoscopic-loss mechanism and its propagation characteristics, namely, velocity dispersion and quality factor. The approach requires the introduction of a first-order in time memory-variable equation. Snapshots and time histories are obtained by solving the equations of motion with a direct grid algorithm based on the Fourier pseudospectral method for computing the spatial derivatives (e.g., Carcione, 2014). An example of wave propagation in a sandstone illustrates the potentialities of the theory and simulation algorithm.

Uniform-porosity equations

The double-porosity medium is composed of a background medium (frame) with embedded spherical inclusions made of the same mineral as the frame (but different porosity) and saturated with the same fluid. A list of symbols and equations of the medium properties are given in Appendix A. Ba et al. (2011) derived the equations for uniform (constant)-porosity. They are given in the following subsections.

Strain-displacement relations

$$\epsilon_{ij} = \frac{1}{2}(\partial_i u_j + \partial_j u_i), \quad \epsilon = \epsilon_{ii}, \quad \eta_m = \partial_i U_i^{(m)}, \quad i = 1,2,3, \quad m = 1,2 \tag{1}$$

Stress-strain relations

$$\begin{aligned} \tau_{ij} &= 2\mu\epsilon_{ij} + [A\epsilon + Q_1(\eta_1 + \phi_2\zeta) + Q_2(\eta_2 - \phi_1\zeta)]\delta_{ij}, \\ \sigma_m &= Q_m\epsilon + R_m(\eta_m + \phi_{3-m}\zeta), \end{aligned} \tag{2}$$

Equations of momentum conservation

$$\begin{aligned} &\rho_{00}\ddot{u}_i + \rho_{01}\ddot{U}_i^{(1)} + \rho_{02}\ddot{U}_i^{(2)} + b_1[\dot{u}_i - \dot{U}_i^{(1)}] + b_2[\dot{u}_i - \dot{U}_i^{(2)}] = \partial_j\tau_{ij}, \\ &\rho_{0m}\ddot{u}_i + \rho_{mm}\ddot{U}_i^{(m)} - b_m[\dot{u}_i - \dot{U}_i^{(m)}] = \partial_i\sigma_m. \end{aligned} \tag{3}$$

Biot-Rayleigh equation

$$\begin{aligned} &\tfrac{1}{3}R_0^2\phi_1^2\phi_2\phi_{20}\left(\frac{\rho_f}{\phi_{10}}\ddot{\zeta} - \frac{\eta}{\kappa_1}\dot{\zeta}\right) = \\ &(\phi_2 Q_1 - \phi_1 Q_2)\epsilon + (\phi_2 R_1\eta_1 - \phi_1 R_2\eta_2) + (\phi_2^2 R_1 + \phi_1^2 R_2)\zeta. \end{aligned} \tag{4}$$

The above formulation is obtained from Lagrange's equations based on the strain and kinetic energies and dissipation potential, associated with the local fluid flow motion described by a generalization of Rayleigh's theory of liquid collapse of a spherical cavity.

2D equations. Particle velocity-stress formulation

Assuming propagation in the (x, z)-plane:

Rate of strain-velocity relations

$$\begin{array}{l} \dot{\epsilon} = \dot{\epsilon}_{xx} + \dot{\epsilon}_{zz}, \\ \dot{\epsilon}_{xx} = \partial_x v_x, \quad \dot{\epsilon}_{zz} = \partial_z v_z, \\ 2\dot{\epsilon}_{xz} = \partial_x v_z + \partial_z v_x, \\ \dot{\eta}_1 = \partial_x V_x^{(1)} + \partial_z V_z^{(1)}, \\ \dot{\eta}_2 = \partial_x V_x^{(2)} + \partial_z V_z^{(2)}. \end{array} \tag{5}$$

Rate of stress-rate of strain relations

$$\begin{array}{l} \dot{\tau}_{xx} = 2\mu\dot{\epsilon}_{xx} + A\dot{\epsilon} + Q_1(\dot{\eta}_1 + \phi_2\dot{\zeta}) + Q_2(\dot{\eta}_2 - \phi_1\dot{\zeta}), \\ \dot{\tau}_{zz} = 2\mu\dot{\epsilon}_{zz} + A\dot{\epsilon} + Q_1(\dot{\eta}_1 + \phi_2\dot{\zeta}) + Q_2(\dot{\eta}_2 - \phi_1\dot{\zeta}), \\ \dot{\sigma}_1 = Q_1\dot{\epsilon} + R_1(\dot{\eta}_1 + \phi_2\dot{\zeta}), \\ \dot{\sigma}_2 = Q_2\dot{\epsilon} + R_2(\dot{\eta}_2 - \phi_1\dot{\zeta}), \\ \dot{\tau}_{xz} = 2\mu\dot{\epsilon}_{xz}. \end{array} \tag{6}$$

Equations of momentum conservation

For each component $i = x, z$, we have

$$\begin{pmatrix} \rho_{00} & \rho_{01} & \rho_{02} \\ \rho_{01} & \rho_{11} & 0 \\ \rho_{02} & 0 & \rho_{22} \end{pmatrix} \begin{pmatrix} \dot{v}_i \\ \dot{V}_i^{(1)} \\ \dot{V}_i^{(2)} \end{pmatrix} = \begin{pmatrix} \partial_x\tau_{ix} + \partial_z\tau_{iz} - b_1[v_i - V_i^{(1)}] - b_2[v_i - V_i^{(2)}] \\ \partial_i\sigma_1 + b_1[v_i - V_i^{(1)}] \\ \partial_i\sigma_2 + b_2[v_i - V_i^{(2)}] \end{pmatrix} \equiv \begin{pmatrix} \Pi_i \\ \Pi_i^{(1)} \\ \Pi_i^{(2)} \end{pmatrix} \tag{7}$$

or

$$\begin{pmatrix} \dot{v}_i \\ \dot{V}_i^{(1)} \\ \dot{V}_i^{(2)} \end{pmatrix} = \frac{1}{D} \begin{pmatrix} \rho_{11}\rho_{22} & -\rho_{01}\rho_{22} & -\rho_{02}\rho_{11} \\ -\rho_{01}\rho_{22} & \rho_{00}\rho_{22} - \rho_{02}^2 & \rho_{01}\rho_{02} \\ -\rho_{02}\rho_{11} & \rho_{01}\rho_{02} & \rho_{00}\rho_{11} - \rho_{01}^2 \end{pmatrix} \begin{pmatrix} \Pi_i \\ \Pi_i^{(1)} \\ \Pi_i^{(2)} \end{pmatrix}, \tag{8}$$

$$D = \rho_{00}\rho_{11}\rho_{22} - \rho_{11}\rho_{02}^2 - \rho_{22}\rho_{01}^2.$$

Biot-Rayleigh equation

A velocity-stress formulation would require the additional variables χ and ψ, such that

$$\dot{\zeta} = \chi, \quad \dot{\chi} = \psi, \quad \dot{\psi} = \frac{\phi_{10}\eta}{\rho_f \kappa_1}\psi + \frac{3\phi_{10}}{R_0^2 \rho_f \phi_1^2 \phi_2 \phi_{20}} \dot{\mathcal{F}}, \tag{9}$$

where

$$\dot{\mathcal{F}} = (\phi_2 Q_1 - \phi_1 Q_2)\dot{\epsilon} + (\phi_2 R_1 \dot{\eta}_1 - \phi_1 R_2 \dot{\eta}_2) + (\phi_2^2 R_1 + \phi_1^2 R_2)\chi. \tag{10}$$

However, this equation can be perfectly approximated by the more simple viscoelastic memory-variable equation, as we show in the example.

Approximation with the Zener mechanical model

We approximate the mesoscopic Biot-Rayleigh peak with that of a Zener model (e.g., Carcione, 2014). First, we take $R_0 = \infty$ in equation (9) to uncouple the BR equation from the others. The first two equations (6) can be re-written as

$$\begin{aligned} \dot{\tau}_{xx} &= K\dot{\epsilon} + \frac{2}{3}\mu(2\dot{\epsilon}_{xx} - \dot{\epsilon}_{zz}) + Q_1\dot{\eta}_1 + Q_2\dot{\eta}_2, \\ \dot{\tau}_{zz} &= K\dot{\epsilon} + \frac{2}{3}\mu(2\dot{\epsilon}_{zz} - \dot{\epsilon}_{xx}) + Q_1\dot{\eta}_1 + Q_2\dot{\eta}_2, \end{aligned} \tag{11}$$

where $K = A + (2/3)\mu$. Then, we generalize this modulus to the viscoelastic case as

$$K \to K_\infty \cdot \frac{\tau_\epsilon^{-1} + \mathrm{i}\omega}{\tau_\sigma^{-1} + \mathrm{i}\omega}, \tag{12}$$

where the τ's are relaxation times:

$$\tau_\sigma = \frac{\tau_0}{Q_0}\left(\sqrt{1 + Q_0^2} - 1\right), \quad \tau_\epsilon = \tau_\sigma + \frac{2\tau_0}{Q_0}, \tag{13}$$

where $\tau_0 = 1/(2\pi f_0)$, f_0 is the peak frequency of the BR relaxation mechanism and Q_0 is the minimum quality factor at f_0 [the Fourier convention is $\exp(+\mathrm{i}\omega t)$]. At the low-frequency limit we have $K \to K_0 = K_\infty \tau_\sigma/\tau_\epsilon$.

In the time domain, we have

$$\begin{aligned}\dot{\tau}_{xx} &= \dot{K} * \dot{\epsilon} + \frac{2}{3}\mu(2\dot{\epsilon}_{xx} - \dot{\epsilon}_{zz}) + Q_1\dot{\eta}_1 + Q_2\dot{\eta}_2,\\ \dot{\tau}_{zz} &= \dot{K} * \dot{\epsilon} + \frac{2}{3}\mu(2\dot{\epsilon}_{zz} - \dot{\epsilon}_{xx}) + Q_1\dot{\eta}_1 + Q_2\dot{\eta}_2,\end{aligned} \tag{14}$$

where "$*$" is the time convolution and K is the relaxation function

$$K(t) = K_0 \left[1 - \left(1 - \frac{\tau_\epsilon}{\tau_\sigma}\right)\exp(-t/\tau_\sigma)\right] H(t), \tag{15}$$

where $H(t)$ is the Heaviside step function (Carcione, 2014). We generalize the bulk modulus such that the shear wave is not affected, as in the BR case. The basic elastic deformations of a medium are dilatational and shear, determined by K and μ. A P-wave is a combination of both while the shear waves solely depend on μ (see Carcione, 2014; Section 4.1.2).

Following Carcione (2014, Section 2.10.3), we obtain the memory-variable equation

$$\dot{e} = \left(\frac{1}{\tau_\epsilon} - \frac{1}{\tau_\sigma}\right)\dot{\theta} - \frac{1}{\tau_\sigma}e, \tag{16}$$

for $e = K_\infty^{-1}\dot{K} * \dot{\theta}$ and a given function θ. The complete set of rate of stress-rate of strain relations is then

$$\begin{aligned}\dot{\tau}_{xx} &= K_\infty(\dot{\epsilon} + e) + \frac{2}{3}\mu(2\dot{\epsilon}_{xx} - \dot{\epsilon}_{zz}) + Q_1\dot{\eta}_1 + Q_2\dot{\eta}_2,\\ \dot{\tau}_{zz} &= K_\infty(\dot{\epsilon} + e) + \frac{2}{3}\mu(2\dot{\epsilon}_{xx} - \dot{\epsilon}_{zz}) + Q_1\dot{\eta}_1 + Q_2\dot{\eta}_2,\\ \dot{\sigma}_1 &= Q_1\dot{\epsilon} + R_1\dot{\eta}_1,\\ \dot{\sigma}_2 &= Q_2\dot{\epsilon} + R_2\dot{\eta}_2,\\ \dot{\tau}_{xz} &= 2\mu\dot{\epsilon}_{xz},\\ \dot{e} &= \left(\frac{1}{\tau_\epsilon} - \frac{1}{\tau_\sigma}\right)\dot{\epsilon} - \frac{1}{\tau_\sigma}e,\end{aligned} \tag{17}$$

where $K_\infty = K_0\tau_\epsilon/\tau_\sigma$ is the unrelaxed modulus.

Non-uniform-porosity equations

The Lagrangian formulation used by Ba et al. (2011), and consequently the differential equations, hold for uniform porosity, since the average displacements of the solid and fluid phases are used as Lagrangian coordinates and the respective stress components are used as generalized forces. These equations are analogous to Biot's 1956 equations describing wave propagation in a two-phase porous medium (Biot, 1956), which hold for constant porosity. The equations for variable porosity were derived by Biot in 1962 (Biot, 1962) where he proposed the displacements of the matrix and the variation of fluid content as generalized coordinates. In this more general case, the corresponding generalized forces are the total stress components and the fluid pressure. The equations in Biot (1962) are the correct ones for describing wave propagation in an inhomogeneous medium, because they are consistent with Darcy's law and the boundary conditions at interfaces separating media with different properties. Here we derive the variable-porosity equations using a method employed by Carcione et al (2003) (see also Carcione, 2014). For completeness, the Lagrangian of the system, expressed in terms of the variation of fluid content, is given in Appendix B.

We introduce the variation of fluid content as the divergence of the relative displacement vector:

$$\xi_m = -\mathrm{div}\ \mathbf{w}^{(m)}, \quad \mathbf{w}^{(m)} = \phi_m(\mathbf{U}^{(m)} - \mathbf{u}), \quad m = 1, 2, \tag{18}$$

which for uniform porosity becomes

$$\xi_m = -\phi_m(\eta_m - \epsilon), \quad m = 1, 2. \tag{19}$$

Defining $\sigma_{ij} = \tau_{ij} + (\sigma_1 + \sigma_2)\delta_{ij}$, $\sigma_m = -\phi_m p_{fm}$, and substituting $\eta_m = \epsilon - \xi_m/\phi_m$ into equations (1)-(4), we obtain:

Strain-displacement relations

$$\begin{aligned}
&\epsilon = \epsilon_{xx} + \epsilon_{yy} + \epsilon_{zz},\\
&\epsilon_{xx} = \partial_x u_x, \quad \epsilon_{yy} = \partial_y u_y, \quad \epsilon_{zz} = \partial_z u_z,\\
&2\epsilon_{xy} = \partial_x u_y + \partial_y u_x,\\
&2\epsilon_{xz} = \partial_x u_z + \partial_z u_x,\\
&2\epsilon_{yz} = \partial_y u_z + \partial_z u_y,\\
&-\xi_1 = \partial_x w_x^{(1)} + \partial_y w_y^{(1)} + \partial_z w_z^{(1)},\\
&-\xi_2 = \partial_x w_x^{(2)} + \partial_y w_y^{(2)} + \partial_z w_z^{(2)}.
\end{aligned} \tag{20}$$

Stress-strain relations

$$\begin{aligned}
&\sigma_{xx} = 2\mu\epsilon_{xx} + \lambda_c\epsilon - \alpha_1 M_1(\xi_1 - \phi_1\phi_2\zeta) - \alpha_2 M_2(\xi_2 + \phi_1\phi_2\zeta),\\
&\sigma_{yy} = 2\mu\epsilon_{yy} + \lambda_c\epsilon - \alpha_1 M_1(\xi_1 - \phi_1\phi_2\zeta) - \alpha_2 M_2(\xi_2 + \phi_1\phi_2\zeta),\\
&\sigma_{zz} = 2\mu\epsilon_{zz} + \lambda_c\epsilon - \alpha_1 M_1(\xi_1 - \phi_1\phi_2\zeta) - \alpha_2 M_2(\xi_2 + \phi_1\phi_2\zeta),\\
&p_{f1} = -\alpha_1 M_1\epsilon + M_1(\xi_1 - \phi_1\phi_2\zeta),\\
&p_{f2} = -\alpha_2 M_2\epsilon + M_2(\xi_2 + \phi_1\phi_2\zeta),\\
&\sigma_{xy} = 2\mu\epsilon_{xy},\\
&\sigma_{xz} = 2\mu\epsilon_{xz},\\
&\sigma_{yz} = 2\mu\epsilon_{yz}.
\end{aligned} \tag{21}$$

Equations of momentum conservation

$$\begin{aligned}
&\rho\ddot{u}_x + \rho_f\ddot{w}_x^{(1)} + \rho_f\ddot{w}_x^{(2)} = \partial_x\sigma_{xx} + \partial_y\sigma_{xy} + \partial_z\sigma_{xz},\\
&\rho\ddot{u}_y + \rho_f\ddot{w}_y^{(1)} + \rho_f\ddot{w}_y^{(2)} = \partial_x\sigma_{xy} + \partial_y\sigma_{yy} + \partial_z\sigma_{yz},\\
&\rho\ddot{u}_z + \rho_f\ddot{w}_z^{(1)} + \rho_f\ddot{w}_z^{(2)} = \partial_x\sigma_{xz} + \partial_y\sigma_{yz} + \partial_z\sigma_{zz},\\
&\rho_f\ddot{u}_x + m_1\ddot{w}_x^{(1)} + \frac{b_1}{\phi_1^2}\dot{w}_x^{(1)} = -\partial_x p_{f1},\\
&\rho_f\ddot{u}_y + m_1\ddot{w}_y^{(1)} + \frac{b_1}{\phi_1^2}\dot{w}_y^{(1)} = -\partial_y p_{f1},\\
&\rho_f\ddot{u}_z + m_1\ddot{w}_z^{(1)} + \frac{b_1}{\phi_1^2}\dot{w}_z^{(1)} = -\partial_z p_{f1},\\
&\rho_f\ddot{u}_x + m_2\ddot{w}_x^{(2)} + \frac{b_2}{\phi_2^2}\dot{w}_x^{(2)} = -\partial_x p_{f2},\\
&\rho_f\ddot{u}_y + m_2\ddot{w}_y^{(2)} + \frac{b_2}{\phi_2^2}\dot{w}_y^{(2)} = -\partial_y p_{f2},\\
&\rho_f\ddot{u}_z + m_2\ddot{w}_z^{(2)} + \frac{b_2}{\phi_2^2}\dot{w}_z^{(2)} = -\partial_z p_{f2}.
\end{aligned} \tag{22}$$

Biot-Rayleigh equation

$$\begin{aligned}&\phi_{20}R_0^2[\rho_f\phi_1\ddot{\zeta}-b_1\dot{\zeta}]=\\&3\phi_{10}[(\alpha_1M_1-\alpha_2M_2)\epsilon+(M_2\xi_2-M_1\xi_1)+\phi_1\phi_2(M_1+M_2)\zeta].\end{aligned}\tag{23}$$

Approximation with the Zener mechanical model

As in the uniform-porosity case, we approximate the mesoscopic Biot-Rayleigh peak with that of a Zener model if we take $R_0\to\infty$. In this case the Gassmann modulus $K_G=\lambda_c+2\mu/3$ becomes

$$K_G\to K_{G\infty}\cdot\frac{\tau_\epsilon^{-1}+\mathrm{i}\omega}{\tau_\sigma^{-1}+\mathrm{i}\omega},\tag{24}$$

and we have $K_{G0}=K_{G\infty}\tau_\sigma/\tau_\epsilon$.

We present here the 2D equations; the 3D equations are a straightforward generalization. Assuming propagation in the (x,z)-plane, the stress-strain equations (21) can be re-written as

$$\begin{aligned}\sigma_{xx}&=K_G\epsilon+\frac{2}{3}\mu(2\epsilon_{xx}-\epsilon_{zz})-\alpha_1M_1\xi_1-\alpha_2M_2\xi_2,\\\sigma_{zz}&=K_G\epsilon+\frac{2}{3}\mu(2\epsilon_{zz}-\epsilon_{xx})-\alpha_1M_1\xi_1-\alpha_2M_2\xi_2,\\p_{f1}&=M_1(\xi_1-\alpha_1\epsilon),\\p_{f2}&=M_2(\xi_2-\alpha_2\epsilon),\\\sigma_{xz}&=2\mu\epsilon_{xz}.\end{aligned}\tag{25}$$

where we have highlighted $K_G=\lambda_c+2\mu/3$, which becomes complex and frequency-dependent when replaced by the Zener kernel. We generalize the Gassmann bulk modulus such that the shear wave is not affected, as in the BR case.

Following the same procedure of the preceding section, the equations of motion in the velocity-stress formulation, with memory variable, are:

Rate of strain-velocity relations

$$\begin{aligned}
&\dot{\epsilon} = \dot{\epsilon}_{xx} + \dot{\epsilon}_{zz}, \\
&\dot{\epsilon}_{xx} = \partial_x v_x, \quad \dot{\epsilon}_{zz} = \partial_z v_z, \\
&2\dot{\epsilon}_{xz} = \partial_x v_z + \partial_z v_x, \\
&-\dot{\xi}_1 = \partial_x q_x^{(1)} + \partial_z q_z^{(1)}, \\
&-\dot{\xi}_2 = \partial_x q_x^{(2)} + \partial_z q_z^{(2)}.
\end{aligned} \tag{26}$$

Rate of stress-rate of strain relations

$$\begin{aligned}
&\dot{\sigma}_{xx} = K_{G\infty}(\dot{\epsilon} + e) + \frac{2}{3}\mu(2\dot{\epsilon}_{xx} - \dot{\epsilon}_{zz}) - \alpha_1 M_1 \dot{\xi}_1 - \alpha_2 M_2 \dot{\xi}_2, \\
&\dot{\sigma}_{zz} = K_{G\infty}(\dot{\epsilon} + e) + \frac{2}{3}\mu(2\dot{\epsilon}_{zz} - \dot{\epsilon}_{xx}) - \alpha_1 M_1 \dot{\xi}_1 - \alpha_2 M_2 \dot{\xi}_2, \\
&\dot{p}_{f1} = M_1(\dot{\xi}_1 - \alpha_1 \dot{\epsilon}), \\
&\dot{p}_{f2} = M_2(\dot{\xi}_2 - \alpha_2 \dot{\epsilon}), \\
&\dot{\sigma}_{xz} = 2\mu \dot{\epsilon}_{xz}, \\
&\dot{e} = \left(\frac{1}{\tau_\epsilon} - \frac{1}{\tau_\sigma}\right)\dot{\epsilon} - \frac{1}{\tau_\sigma} e,
\end{aligned} \tag{27}$$

where $K_{G\infty} = \lambda_c + 2\mu/3$.

Equations of momentum conservation

For each component $i = x, z$, we have

$$\begin{pmatrix} \rho & \rho_f & \rho_f \\ \rho_f & m_1 & 0 \\ \rho_f & 0 & m_2 \end{pmatrix} \begin{pmatrix} \dot{v}_i \\ \dot{q}_i^{(1)} \\ \dot{q}_i^{(2)} \end{pmatrix} = \begin{pmatrix} \partial_x \sigma_{ix} + \partial_z \sigma_{iz} \\ -\partial_i p_{f1} - \dfrac{b_1}{\phi_1^2} q_i^{(1)} \\ -\partial_i p_{f2} - \dfrac{b_2}{\phi_2^2} q_i^{(2)} \end{pmatrix} \equiv \begin{pmatrix} \Pi_i \\ \Pi_i^{(1)} \\ \Pi_i^{(2)} \end{pmatrix} \tag{28}$$

or

$$D \begin{pmatrix} \dot{v}_i \\ \dot{q}_i^{(1)} \\ \dot{q}_i^{(2)} \end{pmatrix} = \begin{pmatrix} m_1 m_2/\rho_f & -m_2 & -m_1 \\ -m_2 & (\rho m_2/\rho_f - \rho_f) & \rho_f \\ -m_1 & \rho_f & (\rho m_1/\rho_f - \rho_f) \end{pmatrix} \begin{pmatrix} \Pi_i \\ \Pi_i^{(1)} \\ \Pi_i^{(2)} \end{pmatrix}, \tag{29}$$

$$D = m_1 m_2 \rho/\rho_f - \rho_f(m_1 + m_2).$$

The algorithm to solve the wave equation numerically is illustrated in Appendix C.

Results

We consider the properties shown in Table 1. In appendix D, we have performed a plane-wave analysis of the equations of motion, to obtain the phase velocity and dissipation factor of the fast P wave. These quantities are represented in Figure 1, where the dots correspond to the fit of the Zener model with $Q_0 = 6.3$. Two other values of R_0 are considered. It can be seen that increasing R_0 moves the relaxation peaks to the low frequencies. This is the case of uniform porosity. For non-uniform porosity, we generalize the wet-rock Gassmann modulus K_G, such that $A(\omega) = K_G(\omega) - \mathcal{K} - 2\mu/3$, or $\lambda_c(\omega) = K_G(\omega) - 2\mu/3$, and $Q_0 = 6.9$. The fit is equally perfect. The Biot peak can be observed at high frequencies.

The simulations use a $n_x \times n_z = 236 \times 236$ mesh, with a uniform grid spacing $dx = dz = 5$ m. The source is a horizontal force (f_x) and its time history (a Ricker wavelet) is $h(t) = (a - 0.5)\exp(-a)$, $a = [\pi f_p(t - t_s)]^2$, $t_s = 1.4/f_p$, with $f_p = 30$ Hz, the source central frequency. Figure 3 shows the snapshots of the particle-velocity components at 165 ms, with and without the BR attenuation mechanism. At the right panels, the P wave (outer wavefront) has been attenuated compared to the inner wavefront (S wave). Figure 4 shows $q_x^{(2)}$ and $q_z^{(2)}$ for $\eta = 0$. In this case, the slow waves propagate and can be identified as the inner wavefronts (see Ba et al., 2011). Seismograms of the vertical components of the wavefield are shown in Figure 5, where the red line corresponds to the case with BR loss mechanism. P-wave attenuation and velocity dispersion can be appreciated.

The last example considers wave propagation in the presence of a planar interface separating two half spaces. The lower one has the properties of the previous simulation, whereas the upper half space has $\rho_s = 2550$ kg/m^3, $K_s = 20$ GPa and $\mu_s =$

28 GPa and the other properties are the same as those given in Table 1. The phase velocity and quality factor of the upper half space are obtained with $f_0 = 21$ Hz and $Q_0 = 11.9$ Figure 6 shows snapshots of the v_x-wavefield at 165 ms without (a) and with (b) the BR mesoscopic attenuation. The source location is (590, 640) m. Seismograms of the v_x and v_z components at the location (300, 300) m are displayed in Figure 7. The red line corresponds to the case with BR loss mechanism. The P wave is attenuated whereas the S wave is unaffected.

Conclusions

We have developed a numerical algorithm for wave simulation in a double-porosity medium with seismic velocity and attenuation described by the Biot-Rayleigh loss mechanism, where spherical patches or inclusions induce the conversion of fast P-wave energy to slow diffusive modes (the theory predicts two slow modes). The equations for uniform porosity have been generalized to the non-uniform porosity case in order to obtain seismograms in inhomogeneous media. The differential equation of the Biot-Rayleigh field variable is approximated with the Zener mechanical model, which results in a memory-variable viscoelastic equation. The model predicts a relaxation peak in the seismic band, depending on the diameter of the patches, to model the attenuation level observed in rocks.

The algorithm, which is second-order accurate in time and has spectral accuracy in the space variable, allows general material variability and provides snapshots and time histories of the rock-frame and fluid particle velocities and corresponding stress components. Since the presence of slow quasi-static modes makes the differential equations stiff, a time-splitting integration algorithm is used to solve the stiff part analytically.

Acknowledgement: This research is supported by the "National Nature Science Foundation of China (41804095)", the "Fundamental Research Funds for the Central Universities (2019B17614)", the "China Postdoctoral Science Foundation (2017M621618)", the "Specially-appointed Professor Plan of Jiangsu Province, China, and the"open fund of the State Key Laboratory of the Institute of Geodesy and Geophysics, CAS (SKLGED2017-5-2-E)".

References

Ba, J., Carcione, J. M., and Nie, J., 2011, Biot-Rayleigh theory of wave propagation in double-porosity media, Journal of Geophysical Research - Solid earth, 116, B06202.

Biot, M.A., 1956, Theory of propagation of elastic waves in a fluid-saturated porous solid. I. Low-frequency range, J. Acoust. Soc. Am. 28, 168-178.

Biot, M. A., 1962, Mechanics of deformation and acoustic propagation in porous media, J. Appl. Phys., 33, 1482-1498.

Carcione, J. M., 1998, Viscoelastic effective rheologies for modeling wave propagation in porous media, Geophys. Prosp., 46, 249-270.

Carcione, J. M., 2014, Wave Fields in Real Media. Theory and numerical simulation of wave propagation in anisotropic, anelastic, porous and electromagnetic media, Elsevier. (Third edition, extended and revised).

Carcione, J. M., and Quiroga-Goode, G., 1995, Some aspects of the physics and numerical modeling of Biot compressional waves, J. Comput. Acous., 3, 261-280.

Carcione, J. M., Santos, J. E., Ravazzoli, C. L., and Helle, H. B., 2003, Wave simulation in partially frozen porous media with fractal freezing conditions, J. Appl. Phys., 94, 7839-7847.

Carcione, J. M., and Seriani, G., 2001, Wave simulation in frozen porous media, J. Comput. Phys., 170, 676-695.

Müller T., Gurevich B., and Lebedev M., 2010, Seismic wave attenuation and dispersion resulting from wave-induced flow in porous rocks – A review, Geophysics 75, A147-A164.

Picotti, S. and Carcione, J. M., 2017 Numerical simulation of wave-induced fuid flow seismic attenuation based on the Cole-Cole model, J. Acous. Soc. Am., 142, 134-145.

Picotti, S., Carcione, J. M., Rubino, G., Santos, J. E., and Cavallini, F., 2010, A viscoelastic representation of wave attenuation in porous media, Computer & Geosciences, 36, 44-53.

Pride, S. R., Berryman, J. G., and Harris, J. M., 2004, Seismic attenuation due to wave-induced flow, J. Geophys. Res., 109, B01201, 1-19.

Putzer, E. J., 1966, Avoiding the Jordan canonical form in the discussion of linear systems with constant coefficients, Am. Math. Monthly 73, 2.

Santos, J. E., Douglas, Jr., J., Corberó, J. M., and Lovera, O. M., 1990, A model for wave propagation in a porous medium saturated by a two-phase fluid, J. Acoust. Soc. Am., 87, 1439-1448.

Appendix A List of symbols and medium properties

u_i	frame displacement components.
v_i	$= \dot{u}_i$.
m	= 1 (background medium.)
	= 2 (inclusions.)
U_i	fluid displacement components.
V_i	$= \dot{U}_i$.
$w_i^{(m)}$	relative fluid displacement.
$q_i^{(m)}$	$= \dot{w}_i^{(m)}$.
ϵ_{ij}	strain components.
ϵ	solid dilatation.
η_m	divergence of the fluid displacement.
ξ_m	variation of fluid content.
ζ	Biot-Rayleigh variable.
e	memory variable.
τ_{ij}	solid stress components.
σ_m	fluid stress.
σ_{ij}	total stress components.
p_{fm}	fluid pressure.
ϕ_{m0}	porosity.
ν_m	proportion of each medium. $\nu_1 + \nu_2 = 1$.
ϕ_m	$= \nu_m \phi_{m0}$
ϕ	$= \phi_1 + \phi_2$ (total porosity.)
ρ_s	grain density.
ρ_f	fluid density.
K_s	grain bulk modulus.
μ_s	grain shear modulus.
K_f	fluid bulk modulus.
K_{bm}	frame bulk modulus.
μ	frame shear modulus.
λ	dry-rock Lamé constant.
λ_c	wet-rock Lamé constant.
η	fluid viscosity.
κ_m	permeability.
$\mathcal{T}_m$	tortuosity.
R_0	radius of the inclusion.
τ_σ	Zener relaxation time.
τ_ϵ	Zener relaxation time.
f_0	frequency of the relaxation peak.
Q_0	peak quality factor.
P	P-wave modulus.
K	Bulk modulus.
K_0	Low-frequency limit bulk modulus.
K_∞	High-frequency limit bulk modulus.
K_G	Gassmann bulk modulus.
K_{G0}	Gassmann low-frequency limit bulk modulus.
$K_{G\infty}$	Gassmann high-frequency limit bulk modulus.
v_c	complex velocity.
v_p	phase velocity.
α	attenuation factor.
Q	quality factor.

A.1 Medium properties. Constant porosity.

$$\rho_0 = (1-\phi)\rho_s, \quad \rho_1 = \phi_1\rho_f, \quad \rho_2 = \phi_2\rho_f, \quad \rho_{11} = \mathcal{T}_1\phi_1\rho_f, \quad \rho_{22} = \mathcal{T}_2\phi_2\rho_f,$$

$$\rho_{01} = \rho_1 - \rho_{11}, \quad \rho_{02} = \rho_2 - \rho_{22}, \quad \rho = (1-\phi)\rho_s + \phi\rho_f = \rho_0 + \rho_1 + \rho_2,$$

$$\bar{\rho}_1 = \mathcal{T}_1\rho_f/\phi_1, \quad \bar{\rho}_2 = \mathcal{T}_2\rho_f/\phi_2, \quad \rho_{00} = \rho - \phi_1(2\rho_f - \bar{\rho}_1\phi_1) - \phi_2(2\rho_f - \bar{\rho}_2\phi_2),$$

$$\mathcal{T}_m = 0.5(1 + 1/\phi_{m0})],$$

$$A = (1-\phi)K_s - 2\mu/3 - K_s(Q_1+Q_2)/K_f, \quad P = A + 2\mu, \quad K = A + \frac{2}{3}\mu \tag{A.1}$$

$$\beta = \frac{\phi_{20}}{\phi_{10}}\left[\frac{1-(1-\phi_{10})K_s/K_{b1}}{1-(1-\phi_{20})K_s/K_{b2}}\right], \quad \gamma = \frac{K_s}{K_f}\left(\frac{\phi_2+\beta\phi_1}{1-\phi-K_b/K_s}\right),$$

$$\frac{1}{K_b} = \frac{\nu_1}{K_{b1}} + \frac{\nu_2}{K_{b2}}, \quad b_1 = \phi_1\phi_{10}\frac{\eta}{\kappa_1}, \quad b_2 = \phi_2\phi_{20}\frac{\eta}{\kappa_2},$$

$$Q_1 = \frac{\beta\phi_1 K_s}{\beta+\gamma}, \quad Q_2 = \frac{\phi_2 K_s}{1+\gamma}, \quad R_1 = \frac{\phi_1 K_f}{1+\beta/\gamma}, \quad R_2 = \frac{\phi_2 K_f}{1+1/\gamma}.$$

A.2 Medium properties. Variable porosity.

$$\rho = (1-\phi)\rho_s + \phi\rho_f,$$

$$m_m = \frac{\mathcal{T}_m \rho_f}{\phi_m} = \frac{(\phi_m + \nu_m)\rho_f}{2\phi_m^2} \quad [\text{if } \mathcal{T}_m = 0.5(1 + 1/\phi_{m0})],$$

$$\lambda_c = K_b - \frac{2}{3}\mu + F = \lambda + F, \quad K_G = \lambda_c + \frac{2}{3}\mu,$$

$$F = (1-\phi)K_s - K_b + \left(2 - \frac{K_s}{K_f}\right)(\phi_1\alpha_1 M_1 + \phi_2\alpha_2 M_2) - \left(1 - \frac{K_s}{K_f}\right)(\phi_1^2 M_1 + \phi_2^2 M_2),$$

$$\alpha_1 = \phi_1 + \frac{\beta\phi_1 K_s}{\gamma K_f}, \quad \alpha_2 = \phi_2 + \frac{\phi_2 K_s}{\gamma K_f},$$

$$M_1 = \frac{K_f}{\phi_1(1+\beta/\gamma)}, \quad M_2 = \frac{K_f}{\phi_2(1+1/\gamma)},$$

$$Q_m = \phi_m M_m(\alpha_m - \phi_m), \quad R_m = \phi_m^2 M_m, \quad m = 1, 2,$$

$$\mathcal{K} = \lambda_c - A = \phi_1 M_1(2\alpha_1 - \phi_1) + \phi_2 M_2(2\alpha_2 - \phi_2). \tag{A.2}$$

Appendix B Biot-Rayleigh Lagrangian for non-uniform porosity

The basic equations are similar to those derived in Ba et al. (2011), but using the relative fluid displacements, instead of the displacements. It is similar to the difference between the theories given in Biot (1956) and Biot (1962) (see Carcione, 2014). Here, we pay special attention to the derivation of the Biot-Rayleigh equation, which describes the mesoscopic loss. The strain energy, W, is given by

$$\begin{aligned} 2W = {} & (\lambda_c + 2\mu)\epsilon^2 - 2\alpha_1 M_1(\xi_1 - \phi_1\phi_2\zeta)\epsilon - 2\alpha_2 M_2(\xi_2 + \phi_1\phi_2\zeta)\epsilon \\ & + M_1(\xi_1 - \phi_1\phi_2\zeta)^2 + M_2(\xi_2 + \phi_1\phi_2\zeta)^2 - 4\mu I_2, \end{aligned} \tag{B.1}$$

where

$$I_1 = \epsilon_{ii}, \quad I_2 = \begin{vmatrix} \epsilon_{11} & \epsilon_{12} \\ \epsilon_{12} & \epsilon_{22} \end{vmatrix} + \begin{vmatrix} \epsilon_{22} & \epsilon_{23} \\ \epsilon_{23} & \epsilon_{33} \end{vmatrix} + \begin{vmatrix} \epsilon_{33} & \epsilon_{13} \\ \epsilon_{13} & \epsilon_{11} \end{vmatrix}, \quad \begin{vmatrix} \epsilon_{11} & \epsilon_{12} & \epsilon_{13} \\ \epsilon_{12} & \epsilon_{22} & \epsilon_{23} \\ \epsilon_{13} & \epsilon_{23} & \epsilon_{33} \end{vmatrix}, \tag{B.2}$$

ϵ_{ij} denote the strain components of the matrix, ξ_m are the variations of fluid content, as defined by Biot (1962) (see Carcione, 2014), and ζ is the Biot-Rayleigh variable (Ba et al., 2011).

The kinetic energy is

$$2T = \rho \sum_i \dot{u}_i^2 + \rho_f \sum_m \sum_i \left[2\dot{u}_i \dot{w}_i^{(m)} + (\dot{w}_i^{(m)})^2 \right] + 2T_L, \tag{B.3}$$

where

$$T_L = \frac{1}{6} \rho_f R_0^2 \left(\frac{\phi_{20}\phi_1^2\phi_2}{\phi_{10}} \right) \dot{\zeta}^2 \tag{B.4}$$

is the kinetic energy of the inclusions.

The dissipation function, based on Biot's approach (Biot, 1956, 1962), is

$$2D = \sum_m \sum_i b_m \dot{w}_i^{(m)} \dot{w}_i^{(m)} + 2D_L, \tag{B.5}$$

where

$$D_L = \frac{1}{6} \left(\frac{\eta}{\kappa_1} \right) \phi_{20}\phi_1^2\phi_2 R_0^2 \dot{\zeta}^2 \tag{B.6}$$

is the dissipation energy of the inclusions.

Lagrange's equation

$$\partial_t \left(\frac{\partial L}{\partial \dot{\zeta}} \right) + \frac{\partial L}{\partial \zeta} + \frac{\partial D}{\partial \dot{\zeta}} = 0, \tag{B.7}$$

yields the Biot-Rayleigh equation, where

$$L = T - W \tag{B.8}$$

is the Lagrangian. See Appendix A for a detailed list of symbols.

Appendix C The algorithm

The 2D velocity-stress differential equations can be written in matrix form as

$$\dot{\mathbf{v}} = \mathbf{M}\mathbf{v} + \mathbf{s}, \tag{C.1}$$

where

$$\mathbf{v} = [v_x, v_z, q_x^{(1)}, q_z^{(1)}, q_x^{(2)}, q_z^{(2)}, \sigma_{xx}, \sigma_{zz}, \sigma_{xz}, p_{f1}, p_{f2}, e]^\top \tag{C.2}$$

is the unknown velocity-stress vector,

$$\mathbf{s} = [s_x, s_z, 0, 0, 0, 0, 0, 0, 0, 0, 0, 0]^\top \tag{C.3}$$

is the source vector, and $\mathbf{M}$ is the propagation matrix containing the spatial derivatives and material properties. Sources are added in Euler-Newton equations.

The solution to equation (C.1) subject to the initial condition $\mathbf{v}(0) = \mathbf{v}_0$ is formally given by

$$\mathbf{v}(t) = \exp(t\mathbf{M})\mathbf{v}_0 + \int_0^t \exp(\tau\mathbf{M})\mathbf{s}(t-\tau)d\tau, \tag{C.4}$$

where $\exp(t\mathbf{M})$ is called evolution operator.

The eigenvalues of $\mathbf{M}$ have negative real parts and differ greatly in magnitude due to the b_1 and b_2 terms. The presence of large eigenvalues, together with small eigenvalues, indicates that the problem is stiff. The differential equations are solved with the splitting algorithm used by Carcione and Quiroga-Goode (1995). The propagation matrix can be partitioned as

$$\mathbf{M} = \mathbf{M}_r + \mathbf{M}_s, \tag{C.5}$$

where subscript r indicates the regular matrix, and subscript s denotes the stiff matrix, involving the quantities b_1 and b_2. The evolution operator can be expressed as $\exp(\mathbf{M}_r + \mathbf{M}_s)t$. It is easy to show that the product formula

$$\exp(\mathbf{M}dt) = \exp\left(\frac{1}{2}\mathbf{M}_s dt\right)\exp(\mathbf{M}_r dt)\exp\left(\frac{1}{2}\mathbf{M}_s dt\right) \tag{C.6}$$

is second-order accurate in dt. Equation (C.6) allow us to solve the stiff part separately.

The stiff equations, involving the loss parameters b_1 and b_2, are

$$D\begin{pmatrix}\dot{v}_i\\ \dot{q}_i^{(1)}\\ \dot{q}_i^{(2)}\end{pmatrix} = -\begin{pmatrix} m_1 m_2/\rho_f & -m_2 & -m_1\\ -m_2 & (\rho m_2/\rho_f - \rho_f) & \rho_f\\ -m_1 & \rho_f & (\rho m_1/\rho_f - \rho_f)\end{pmatrix}\begin{pmatrix}0\\ (b_1/\phi_1^2)q_i^{(1)}\\ (b_2/\phi_2^2)q_i^{(2)}\end{pmatrix}. \tag{C.7}$$

Let us discretize the time variable as $t = ndt$, where dt is the time step, and denote with a superscript "$*$" the intermediate fields to obtain the solution at $(n+1)dt$ fields from fields at ndt. Equation (C.7) has the subsystem

$$\begin{pmatrix}\dot{q}_i^{(1)}\\ \dot{q}_i^{(2)}\end{pmatrix} = -\frac{1}{D}\begin{pmatrix}(\rho m_2/\rho_f - \rho_f)(b_1/\phi_1^2) & \rho_f(b_2/\phi_2^2)\\ \rho_f(b_1/\phi_1^2) & (\rho m_1/\rho_f - \rho_f)(b_2/\phi_2^2)\end{pmatrix}\begin{pmatrix}q_i^{(1)}\\ q_i^{(2)}\end{pmatrix}, \tag{C.8}$$

or

$$\dot{\mathbf{q}} = \mathbf{A}\ \mathbf{q}, \tag{C.9}$$

whose solution is

$$\mathbf{q}^* = \left[\exp(\lambda_1 dt)\mathbf{I}_2 + \frac{\exp(\lambda_1 dt) - \exp(\lambda_2 dt)}{\lambda_1 - \lambda_2}(\mathbf{A} - \lambda_1 \mathbf{I}_2)\right]\mathbf{q}^n, \tag{C.10}$$

where λ_1 and λ_2 are the eigenvalues of matrix $\mathbf{A}$,

$$2\lambda_{1,2} = a_{11} + a_{22} \pm \sqrt{(a_{11} - a_{22})^2 + 4a_{12}a_{21}}, \tag{C.11}$$

a_{lk} are the components of matrix $\mathbf{A}$ and $\mathbf{I}_2$ is the 2×2 identity matrix (Putzer, 1966). From equation (C.7), we obtain

$$\dot{v}_i = \frac{1}{D}\left(\frac{m_2 b_1}{\phi_1^2}q_i^{(1)} + \frac{m_1 b_2}{\phi_2^2}q_i^{(2)}\right) \equiv a q_i^{(1)} + b q_i^{(2)}. \tag{C.12}$$

Using equation (C.10) we have

$$\dot{v}_i = A\exp(\lambda_1 dt) + B\exp(\lambda_2 dt), \tag{C.13}$$

where

$$A = aq_i^{(1)n} + bq_i^{(2)n} + \frac{1}{\lambda_1 - \lambda_2}\left[aq_i^{(1)n}(a_{11}-\lambda_1) + bq_i^{(2)n}(a_{22}-\lambda_1) + aq_i^{(2)n}a_{12} + bq_i^{(1)n}a_{21}\right],$$
$$B = -\frac{1}{\lambda_1 - \lambda_2}\left[aq_i^{(1)n}(a_{11}-\lambda_1) + bq_i^{(2)n}(a_{22}-\lambda_1) + aq_i^{(2)n}a_{12} + bq_i^{(1)n}a_{21}\right]. \tag{C.14}$$

Equation (C.13) has the solution

$$v_i^* = v_i^n + \frac{A}{\lambda_1}[\exp(\lambda_1 dt) - 1] + \frac{B}{\lambda_2}[\exp(\lambda_2 dt) - 1], \tag{C.15}$$

or

$$v_i^* = v_i^n + a_1 q_i^{(1)n} + a_2 q_i^{(2)n}, \tag{C.16}$$

where

$$\begin{aligned} a_1 &= \frac{b_1}{\lambda_1}[\exp(\lambda_1 dt) - 1] + \frac{c_1}{\lambda_2}[\exp(\lambda_2 dt) - 1], \\ a_2 &= \frac{b_2}{\lambda_1}[\exp(\lambda_1 dt) - 1] + \frac{c_2}{\lambda_2}[\exp(\lambda_2 dt) - 1], \end{aligned} \tag{C.17}$$

with

$$\begin{aligned} b_1 &= a + \frac{1}{\lambda_1 - \lambda_2}[a(a_{11}-\lambda_1) + ba_{21}], \\ b_2 &= b + \frac{1}{\lambda_1 - \lambda_2}[b(a_{22}-\lambda_1) + aa_{12}], \\ c_1 &= a - b_1, \quad c_2 = b - b_2. \end{aligned} \tag{C.18}$$

Then, vector $\mathbf{q}^*$ and v_i^* are input to a second-order time-stepping algorithm (involving matrix $\mathbf{M}_r$), and the spatial derivatives are calculated with the Fourier method by using the FFT (Carcione, 2014). This spatial approximation is infinitely accurate for band-limited periodic functions with cutoff spatial wavenumbers which are smaller than the cutoff wavenumbers of the mesh. Due to the splitting algorithm, the modeling is second-order accurate in the time discretization.

Appendix D Plane-wave analysis

Ba et al (2011) obtained the complex wavenumber, k, of the three wave modes for a plane-wave kernel $\exp[\mathrm{i}(\mathbf{k}\cdot\mathbf{x}-\omega t)]$, where $\mathbf{k}$ is the wavenumber vector. Equation (B1) in Ba et al. (2011) can be expressed as

$$\det(\bar{\mathbf{A}}+\mathbf{B})=0, \quad \bar{\mathbf{A}}=k^2\mathbf{A}, \tag{D.1}$$

where the components of matrices $\mathbf{A}$ and $\mathbf{B}$ are given in equations (B2) and (B3) of Ba et al. (2011) (the sign of η in eq. (B3) should be the opposite).
Using the properties $\det(k^2\mathbf{A})=k^6\det(\mathbf{A})$ and

$$\det(\bar{\mathbf{A}}+\mathbf{B})=\det(\bar{\mathbf{A}})+\det(\mathbf{B})+\mathrm{tr}(\bar{\mathbf{A}}'\mathbf{B})+\mathrm{tr}(\bar{\mathbf{A}}\mathbf{B}'), \quad \bar{\mathbf{A}}'=\bar{\mathbf{A}}^{-1}\det\bar{\mathbf{A}}, \quad \mathbf{B}'=\mathbf{B}^{-1}\det\bar{\mathbf{B}}, \tag{D.2}$$

we obtain the equation

$$k^6\det\mathbf{A}+k^4\det\mathbf{A}\ \mathrm{tr}(\mathbf{A}^{-1}\mathbf{B})+k^2\det\mathbf{B}\ \mathrm{tr}(\mathbf{A}\mathbf{B}^{-1})+\det\mathbf{B}=0, \tag{D.3}$$

which can be solved analytically for k to obtain three complex velocities

$$v_c=\frac{\omega}{k}. \tag{D.4}$$

The phase velocity and quality factor of each wave mode are

$$v_p=\left[\mathrm{Re}\left(\frac{1}{v_c}\right)\right]^{-1} \tag{D.5}$$

and

$$Q=\frac{\mathrm{Re}(v_c^2)}{\mathrm{Im}(v_c^2)}, \tag{D.6}$$

respectively (Carcione, 2014), where we have used the $\exp(+\mathrm{i}\omega t)$ convention.

Table 1. Poro-elastic properties

Background medium

Grain	$\rho_s = 2650$ kg/m^3
	$K_s = 38$ GPa
	$\mu_s = 44$ GPa
Frame	$K_{b1} = (1-\phi_{10})K_s/(1+c_1\phi_{10})$
	$\mu = (1-\phi)\mu_s/(1+c_S\phi)$
	$\phi_{10} = 0.1$
	$\nu_1 = 0.963$
	$c_1 = 10,\ c_S = 10$
	$\kappa_1 = 0.01$ darcy
	$\mathcal{T}_1 = 0.5(1+1/\phi_{10})$
water	$\rho_f = 1040$ kg/m^3
	$K_f = 2.5$ GPa
	$\eta = 0.001$ Pa s

Patch

$K_{b2} = (1-\phi_{20})K_s/(1+c_2\phi_{20})$
$\phi_{20} = 0.3$
$\nu_2 = 1-\nu_1$
$c_2 = 200$
$\kappa_2 = 1$ darcy
$\mathcal{T}_2 = 0.5(1+1/\phi_{20})$
$R_0 = 2.1$ cm

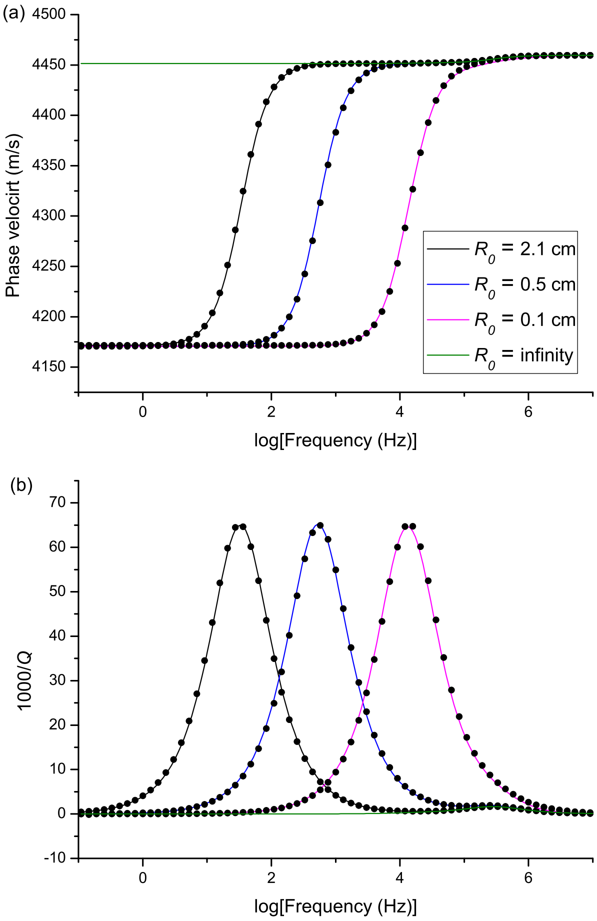

Fig. 1 Phase velocity (a) and dissipation factor (b) of the fast P wave. The dots represent the fit with the Zener model, with $f_0 = 30$ Hz ($R_0 = 2.1$ cm), $f_0 = 10^{2.7}$ Hz ($R_0 = 0.5$ cm), $f_0 = 10^{4.1}$ Hz ($R_0 = 0.1$ cm), and $Q_0 = 6.3$.

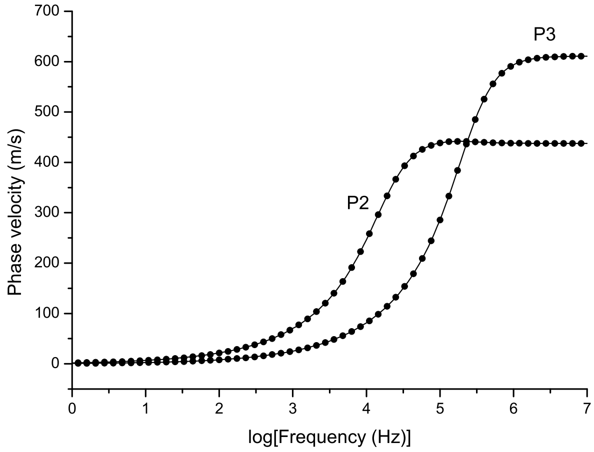

Fig. 2 Phase velocity of the slow P2 (a) and P3 (b) waves. The dots represent a fit with the Zener model, with $f_0 = 30$ Hz and $Q_0 = 6.3$. In this case $R_0 = 2.1$ cm.

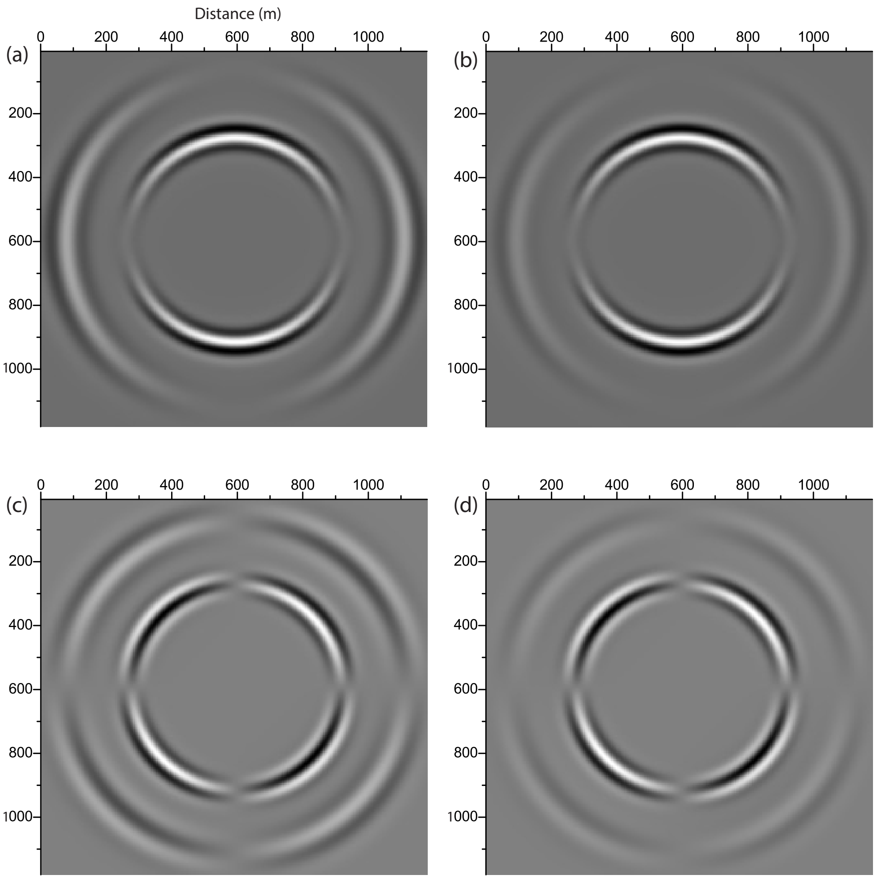

Fig. 3 Snapshots of v_x (a and b) and v_z (c and d) without (a and c) and with (b and d) the BR attenuation peak. The outer and inner wavefronts correspond to the P and S waves, respectively. The numbers express the distance in meters.

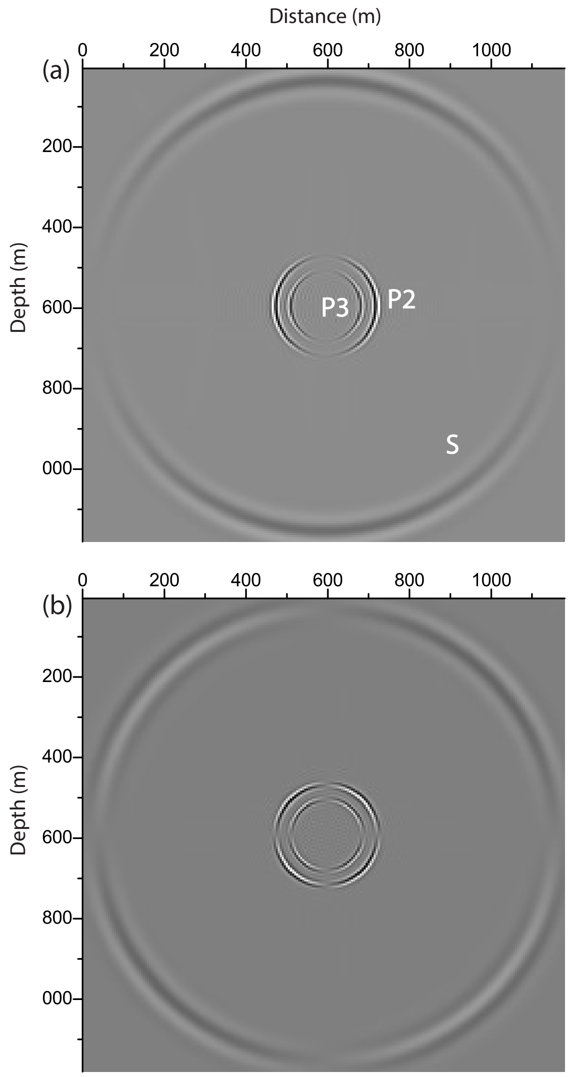

Fig. 4 Snapshots of the $q_x^{(2)}$ (a) and $q_z^{(2)}$ (b) components for $\eta = 0$. The inner wavefronts are the slow waves.

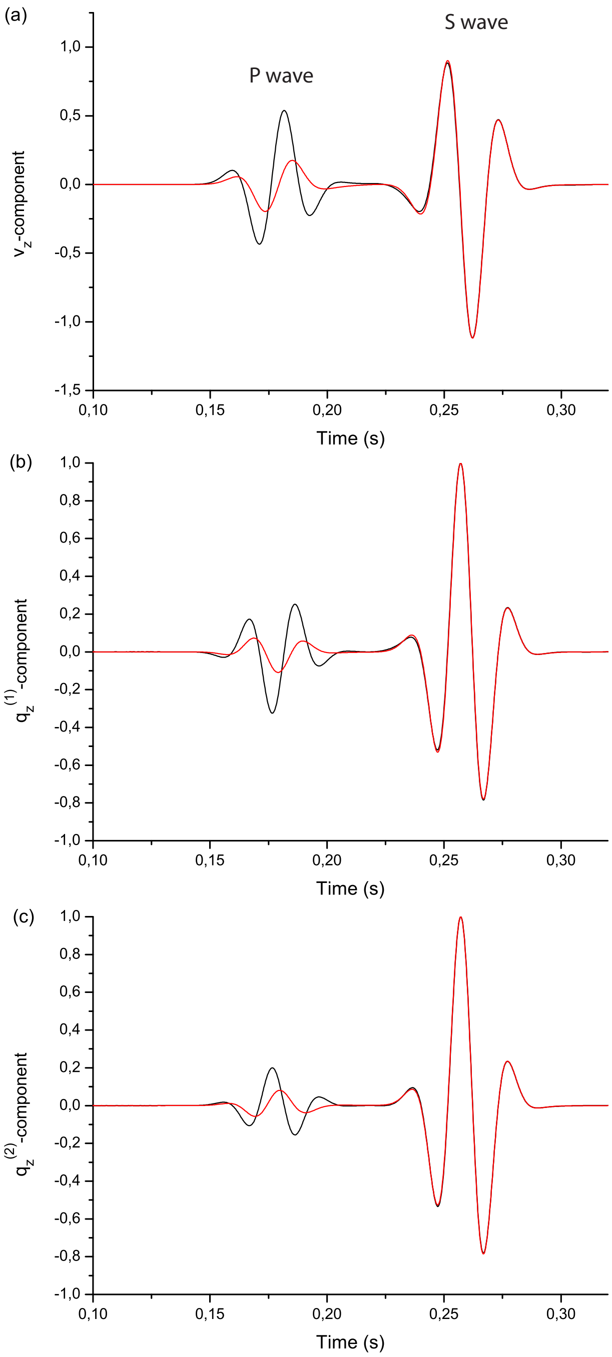

Fig. 5 Seismograms of the v_z, $q_z^{(1)}$ and $q_z^{(2)}$ at the location (150, 200) m. The red line corresponds to the case with BR loss mechanism. The fields are normalised to 1. Actually the fluid particle velocities are smaller by approximately three orders of magnitude.

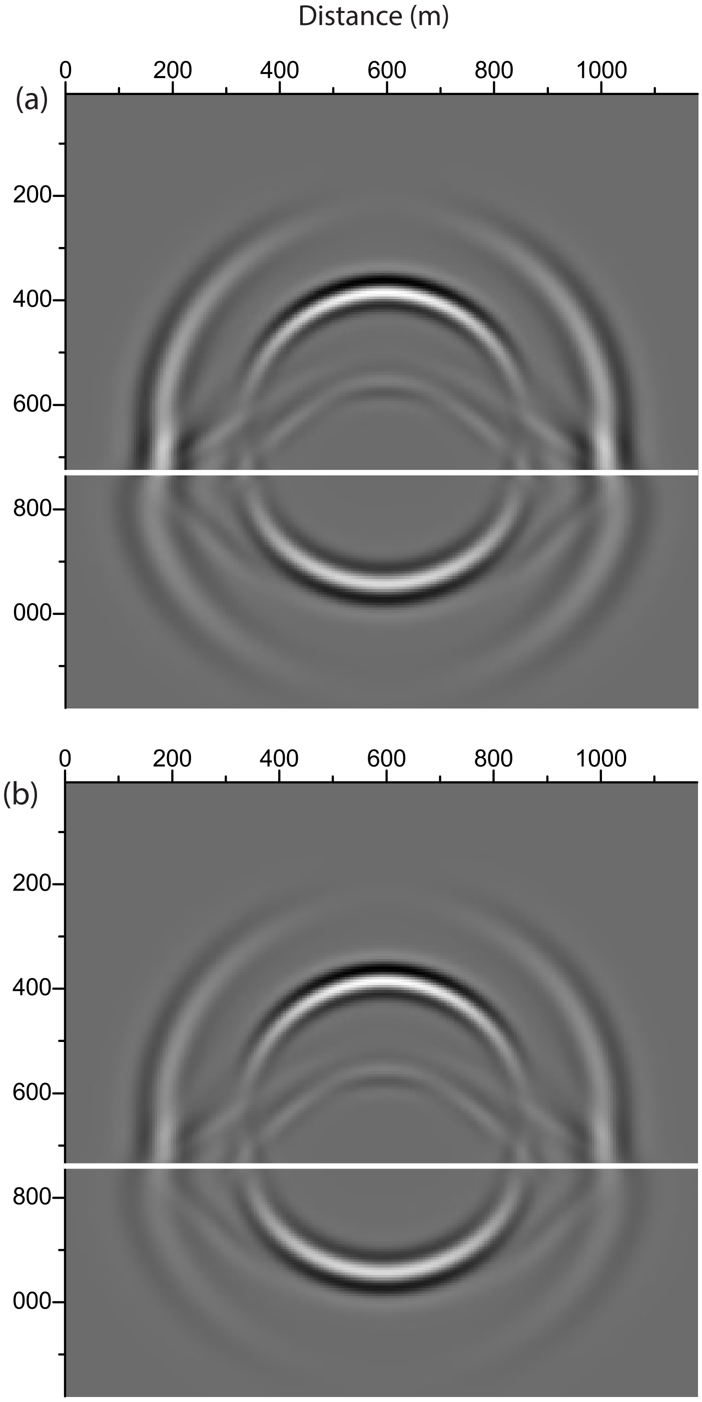

Fig. 6 Flat interface at 740 m (vertical distance) separating two half spaces of dissimilar properties. Snapshots of the v_x-wavefield at 165 ms without (a) and with (b) the BR mesoscopic attenuation.

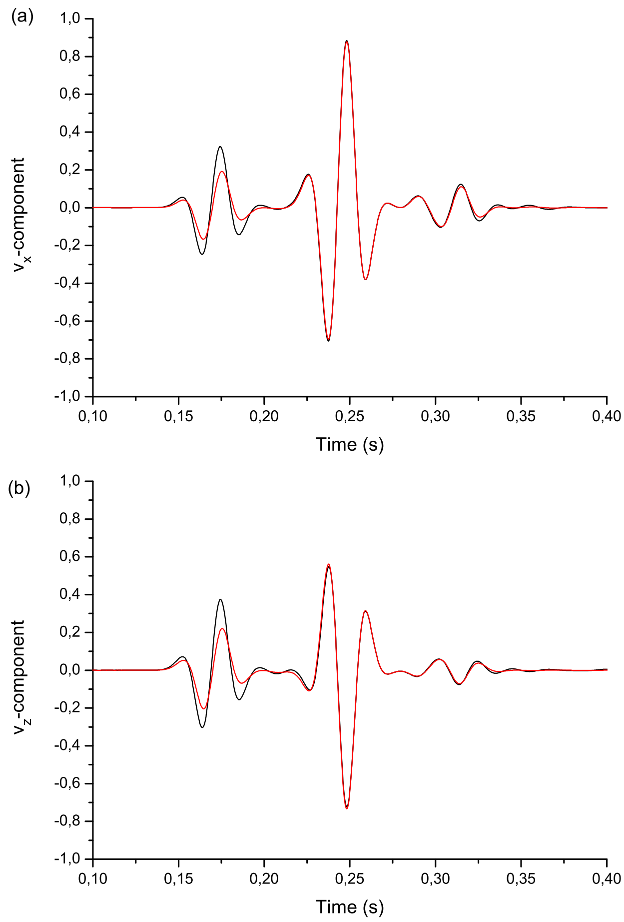

Fig. 7 Seismograms of the v_x and v_z components at the location (300, 300) m. The red line corresponds to the case with BR loss mechanism. The fields are normalized to 1.

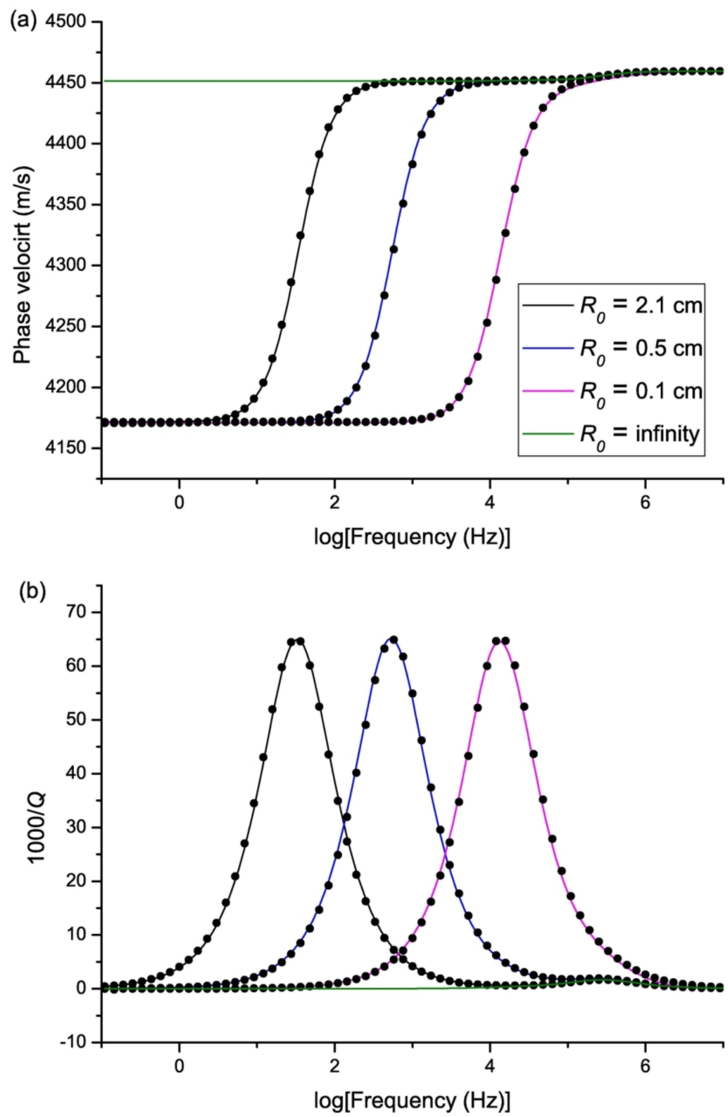

Fig. 1 Phase velocity (a) and dissipation factor (b) of the fast P wave.

144x189mm (300 x 300 DPI)

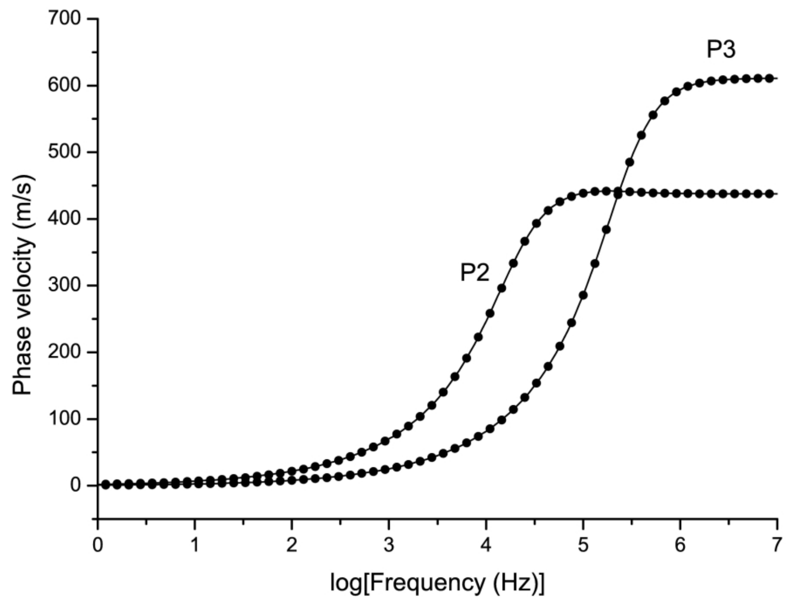

Fig. 2 Phase velocity of the slow P2 (a) and P3 (b) waves.

288x201mm (300 x 300 DPI)

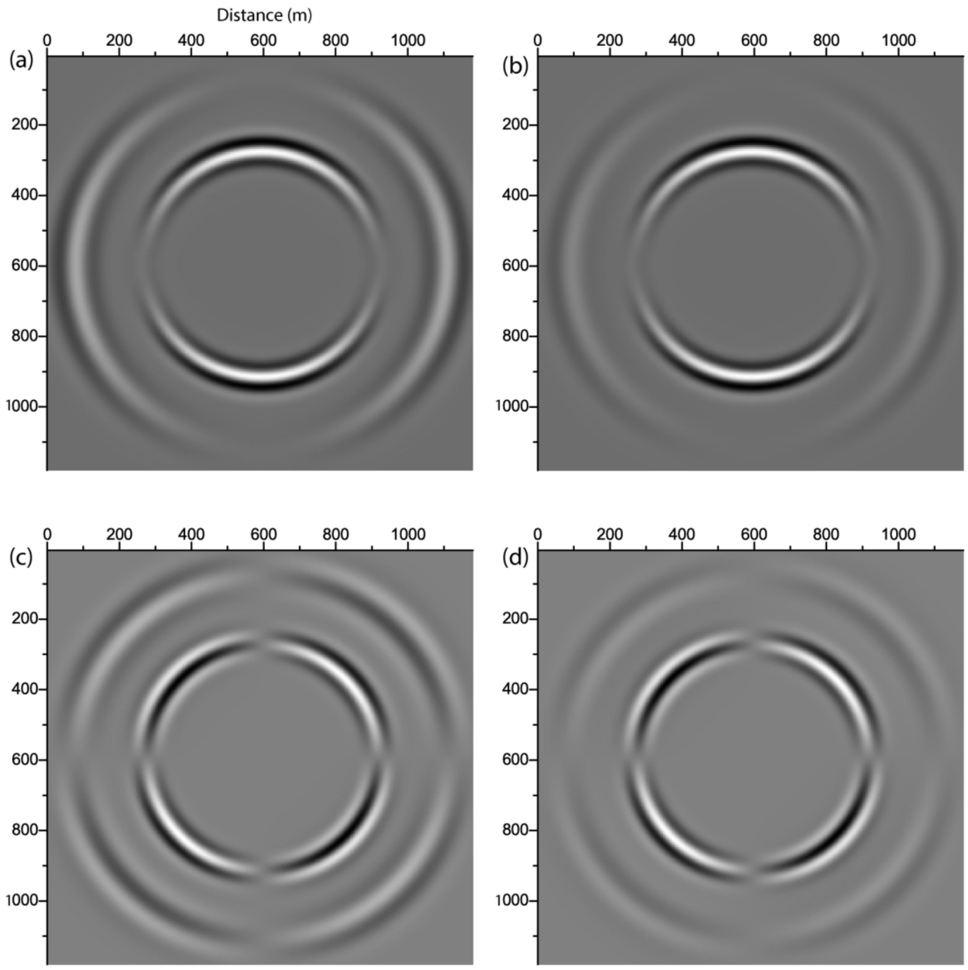

Fig. 3 Snapshots of vx (a and b) and vz (c and d) without (a and c) and with (b and d) the BR attenuation peak. The outer and inner wavefronts correspond to the P and S waves, respectively. The numbers express the distance in meters.

172x173mm (300 x 300 DPI)

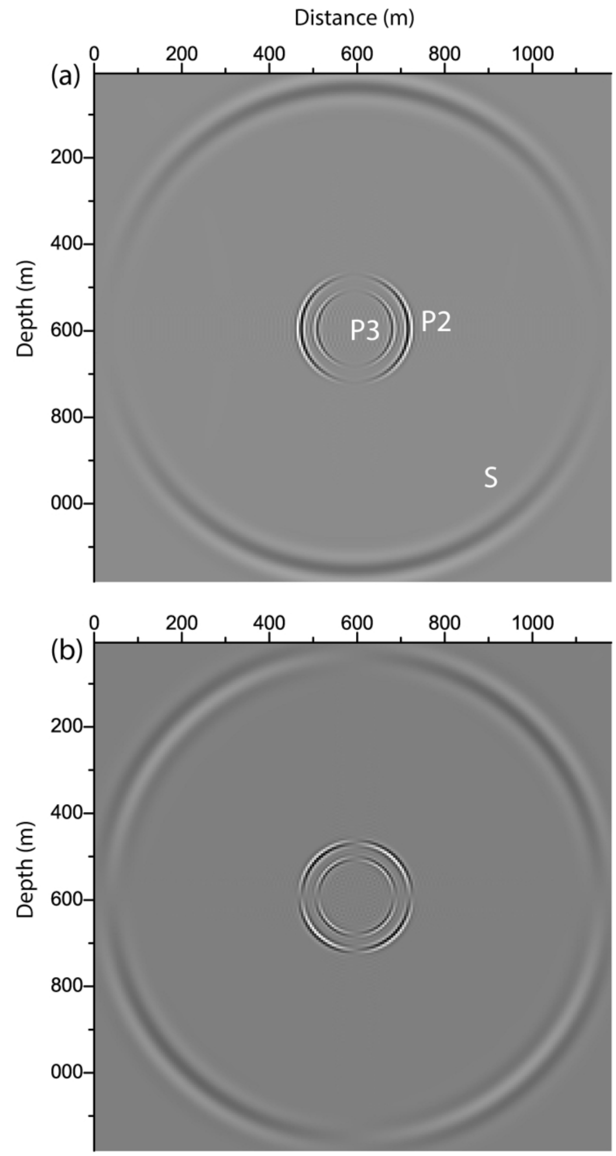

Fig. 4 Snapshots of the q(2)x (a) and q(2)z (b) components for □ = 0. The inner wavefronts are the slow waves.

138x255mm (300 x 300 DPI)

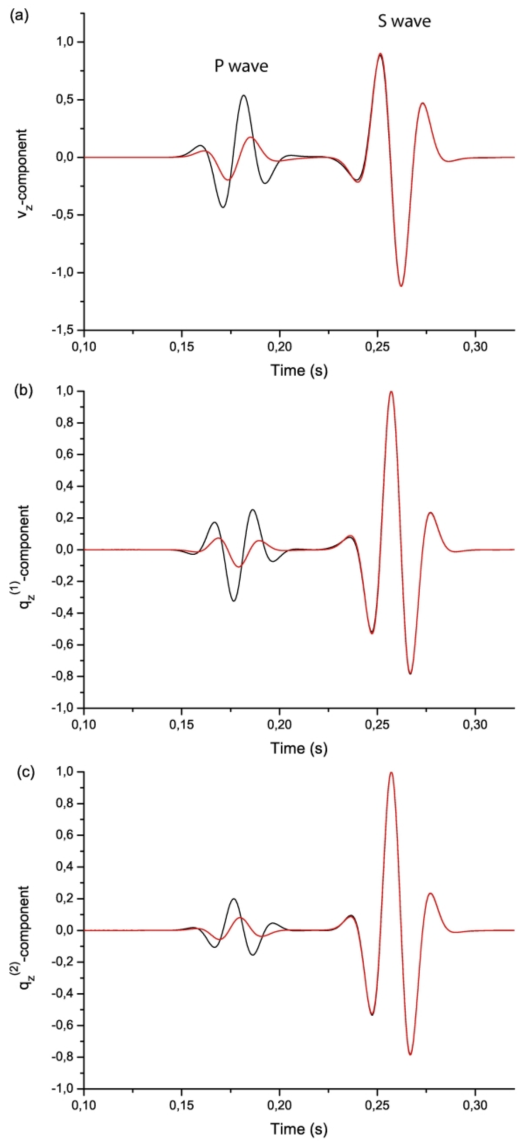

Fig. 5 Seismograms of the vz, q(1) z and q(2) z at the location (150, 200) m. The red line corresponds to the case with BR loss mechanism. The fields are normalised to 1. Actually the fluid particle velocities are smaller by approximately three orders of magnitude.

144x273mm (300 x 300 DPI)

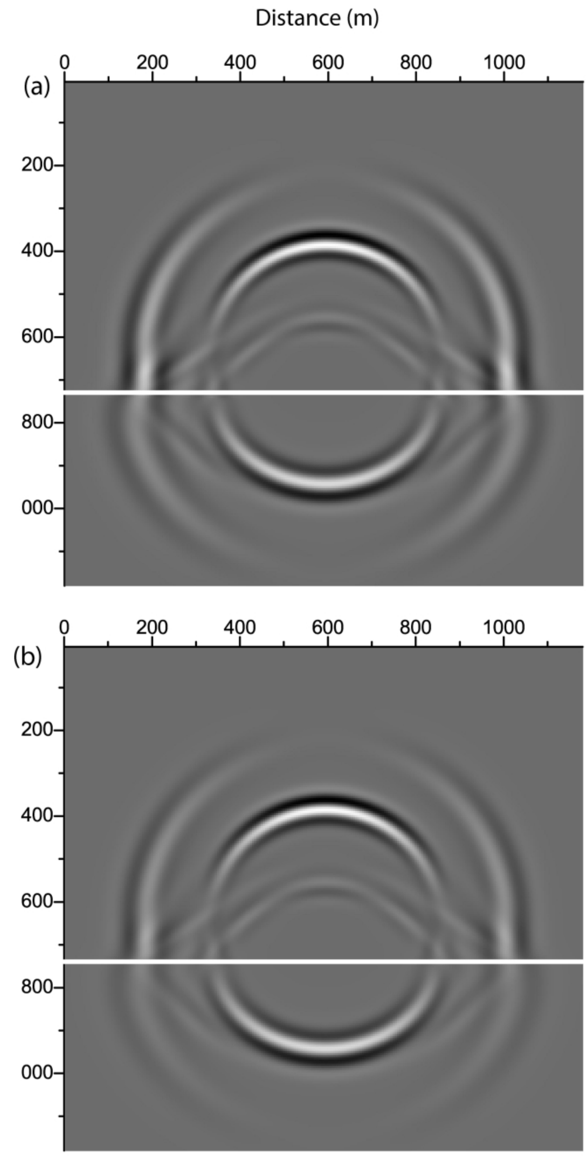

Fig. 6 Flat interface at 740 m (vertical distance) separating two half spaces of dissimilar properties. Snapshots of the vx-wavefield at 165 ms without (a) and with (b) the BR mesoscopic attenuation.

146x283mm (300 x 300 DPI)

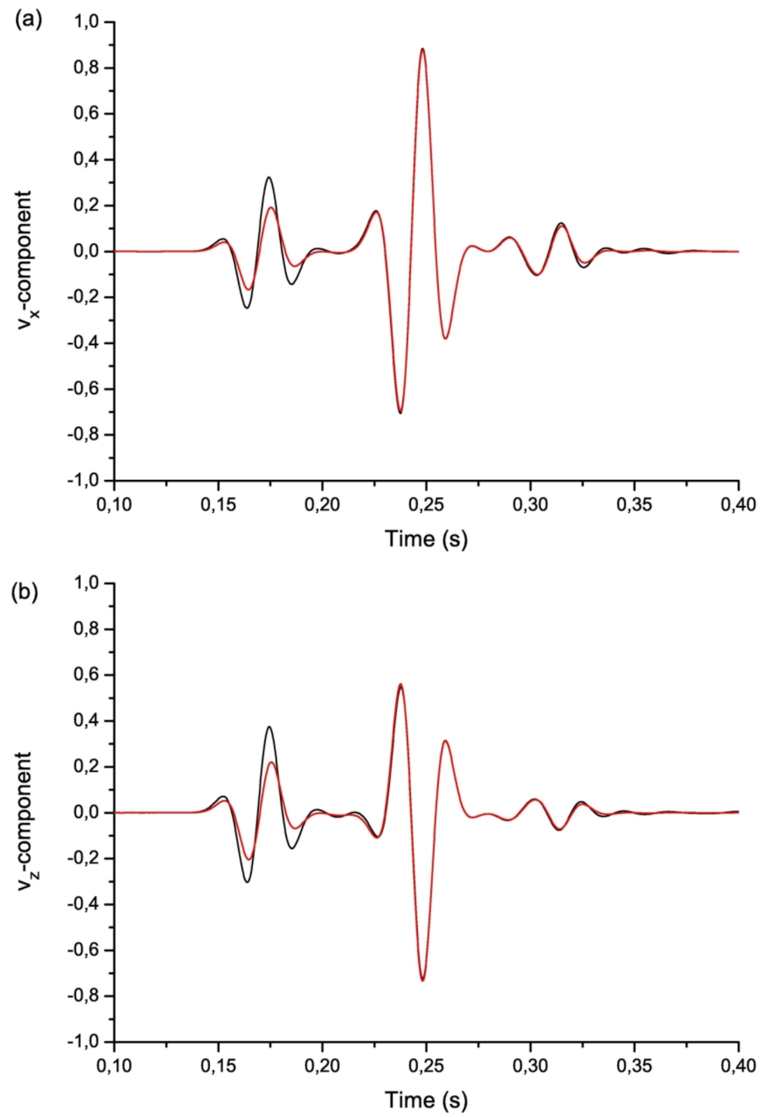

Fig. 7 Seismograms of the vx and vz components at the location (300, 300) m. The red line corresponds to the case with BR loss mechanism. The fields are normalized to 1.

144x189mm (300 x 300 DPI)

DATA AND MATERIALS AVAILABILITY

Data associated with this research are available and can be obtained by contacting the corresponding author.